Research Square

Preprints are preliminary reports that have not undergone peer review.
They should not be considered conclusive, used to inform clinical practice,
or referenced by the media as validated information.

A Geo-AI-Based Framework for Synchronizing Land Use and Land Cover, Thermal Anomalies, and Topographic Wetness: A Comparative Study of Four Cities in Indonesia

Abdul Wahid Hasyim

awahidhs@ub.ac.id

University of Brawijaya

Akhmad Suraji

Andalas University

Ardyanto Tanjung

State University of Malang

Fadhilatus Shoimah

University of Brawijaya

Mohammad Nouval Irfandhia Wahid

Bandung Institute of Technology

Rendyka Achmad Maulidan Firmansyah

University of Brawijaya

Research Article

Keywords: land use and land cover, urban heat island, topographic wetness index, Random Forest, green open space

Posted Date: November 20th, 2026

DOI: https://doi.org/10.21203/rs.3.rs-11570258/v1

License: This work is licensed under a Creative Commons Attribution 4.0 International License.
Read Full License

Additional Declarations: No competing interests reported.

A Geo-AI-Based Framework for Synchronizing Land Use and Land Cover, Thermal Anomalies, and Topographic Wetness: A Comparative Study of Four Cities in Indonesia

Abstract

Uncontrolled expansion of Built-up in Indonesian urban areas has caused the shrinkage of Green Open Space (RTH) and a mismatch between spatial planning documents and actual land use conditions. This study aims to analyze the spatial synchronization among Land Use and Land Cover (LULC), Urban Heat Island (UHI), and Topographic Wetness Index (TWI) as a basis for formulating RTH allocation recommendations in spatial planning documents. The study employs a quantitative approach using Geo-AI technology based on the Random Forest algorithm applied to Sentinel-2A imagery (10 m resolution) for land cover classification (Overall Accuracy 92.50%-94.50% and Kappa 90%-93%), complemented by the calculation of Land Surface Temperature (LST) and the Urban Thermal Field Variance Index (UTFVI) from Landsat 8 OLI/TIRS and Landsat 9 OLI-2/TIRS-2 imagery (30 m resolution) for UHI mapping, as well as TWI analysis, in four cities, namely Malang, Padang, Surakarta, and Yogyakarta. The results show that Yogyakarta and Surakarta are dominated by Built-up (83.83% and 82.74%), whereas Padang and Malang are dominated by Vegetation (85.26% and 50.35%). The highest mean surface temperature was recorded in Yogyakarta (31.56 °C), followed by Malang (25.07 °C) and Surakarta (24.47 °C), while Padang recorded the lowest mean (22.71 °C), with the largest extreme UTFVI area found in Padang (272.32 km²). The TWI analysis shows a dominance of the low class (61%-68%) in all cities. Synchronizing the three parameters produces an RTH allocation priority matrix dominated by the non-priority class, with Built-up as the dominant class in the Priority Scenario I zone in all cities. These findings are expected to serve as a reference for local governments in revising spatial planning policies to realize disaster-resilient cities.

Keywords: land use and land cover; urban heat island; topographic wetness index; Random Forest; green open space

1. Introduction

Urbanization is a global phenomenon that continues to grow massively and has become one of the most significant forms of spatial transformation in the modern era (Kementerian PPN/Bappenas RI, 2025). In Indonesia, this dynamic shows a sharp acceleration, with the urban population share reaching 56.67% in 2020 and projected to surge to 72.9% by 2045 (Dokumen Kebijakan Perkotaan Nasional, 2025). This accelerating transformation from rural to urban areas has serious implications for spatial planning, environmental carrying capacity, and infrastructure sustainability (Bappenas, 2025). Globally, rising population numbers have driven the physical expansion of cities at an excessive pace (Güneralp et al., 2020). Urban areas worldwide have been recorded to expand by up to 9,687 km² per year, a rate five times faster than that of 1970-2010 (Liu et al., 2020; Seto et al., 2011). Based on this trend, urban land cover is estimated to increase by 1.2 million km² by 2030 (Seto et al., 2012). In the national context, the uncontrolled expansion of metropolitan corridors is gradually forming massive mega-urban conurbations (Rustiadi et al., 2021).

The exponential increase in Built-up extent has simultaneously caused a drastic decline in the availability of Green Open Space (RTH) (Güneralp et al., 2020). The reduction of vegetation triggers various chronic ecological problems in urban areas, such as rising surface temperatures, reduced water infiltration capacity into the soil, and amplified risks of hydrometeorological disasters such as floods (Hasyim et al., 2025; Ratnasari et al., 2015). These spatial dynamics are reinforced by the findings of Tiwari & Kanchan (2024), who demonstrated that the massive expansion of Built-up is directly proportional to significant increases in mean and maximum surface temperatures due to the loss of natural vegetation cover. Buildings and infrastructure have modified natural hydrological parameters into environments dominated by impervious surfaces, so that rainwater runoff cannot be fully absorbed and instead burdens the urban drainage network (Hasyim et al., 2024; Isdianto et al., 2025). Furthermore, this land cover transformation acts as a primary catalyst for the emergence of the Urban Heat Island (UHI) phenomenon (Jatayu & Susetyo, 2018). The dominance of concrete and asphalt drives thermal anomalies in which urban temperatures rise sharply above those of the surrounding buffer areas (Sukojo et al., 2025). This extreme heat reduces thermal comfort, increases energy consumption, and raises health risks for urban communities (Takano et al., 2023).

To anticipate this ecological crisis, various planning instruments such as the Regional Spatial Plan (RTRW) have normatively set RTH allocations as a pillar of urban stability (Ratnasari et al., 2015). Designating RTH is crucial, given that spatial mitigation strategies based on green infrastructure (urban greening) are among the most critical interventions for

reducing extreme exposure to the Urban Heat Island (UHI) and improving urban climate resilience (Sharma et al., 2026). Nevertheless, a fundamental weakness of earlier spatial planning systems and research is the high level of discrepancy between spatial designation documents and actual land use conditions (Fadhillah, 2025). Land classified as green zones is often illegally converted into commercial space or residential areas (Refnitasari et al., 2025). This misalignment undermines the function of environmental policy, reducing it to mere legal legitimacy without spatial substance (Hannum et al., 2025). As a comprehensive solution, this study builds a modeling framework that combines Land Surface Temperature (LST) parameters to assess UHI performance and the Topographic Wetness Index (TWI) to simulate hydrological inundation accumulation (Takano et al., 2023). Harmonizing these cross-disciplinary parameters represents a paradigm shift in urban spatial thinking, moving from a purely quantitative simplification of area toward the engineering of functional spatial performance in order to meet Sustainable Development Goal (SDG) 11, namely making cities inclusive, safe, resilient, and sustainable (United Nations, 2021).

Therefore, this study aims to analyze the spatial synchronization among Land Use and Land Cover (LULC), Urban Heat Island (UHI), and Topographic Wetness Index (TWI) conditions. The analysis is carried out through a comparative study of four cities with different characteristics, namely Malang, Padang, Surakarta, and Yogyakarta. The integration of these three parameters specifically focuses on evaluating the functional performance of land cover in mitigating urban heat while controlling the risk of waterlogging. The results of this comparison are expected to provide a strategic foundation for local governments in evaluating spatial planning to realize disaster-resilient cities.

2. Research Method

2.1. *Research Approach*

This study is classified as quantitative research. The quantitative approach is a systematic investigation in the data collection stage in which data can be measured using statistics, computation, or mathematics to identify a phenomenon (Ramdhan, 2021). This study uses several main data sources, namely Sentinel, Landsat, and NASA DEM imagery, with the entire data analysis process executed using cloud computing on the Google Earth Engine platform. In sequence, these three remote sensing datasets were processed to produce specific derived parameters. Sentinel imagery was used to produce land cover classification through the Random Forest algorithm, which was then validated through the LULC Accuracy Assessment stage. Next, Landsat imagery was first processed into Land Surface Temperature to extract Urban Heat Island (UHI) data. Meanwhile, the digital elevation model data from NASA DEM were used to model the Topographic Wetness Index. Once the processing results of the three parameters were obtained, the next step was to perform a spatial overlay. This spatial integration of the three variables ultimately yields the Green Space Allocation Priority as the priority formulation for determining Green Open Space (RTH) allocation.

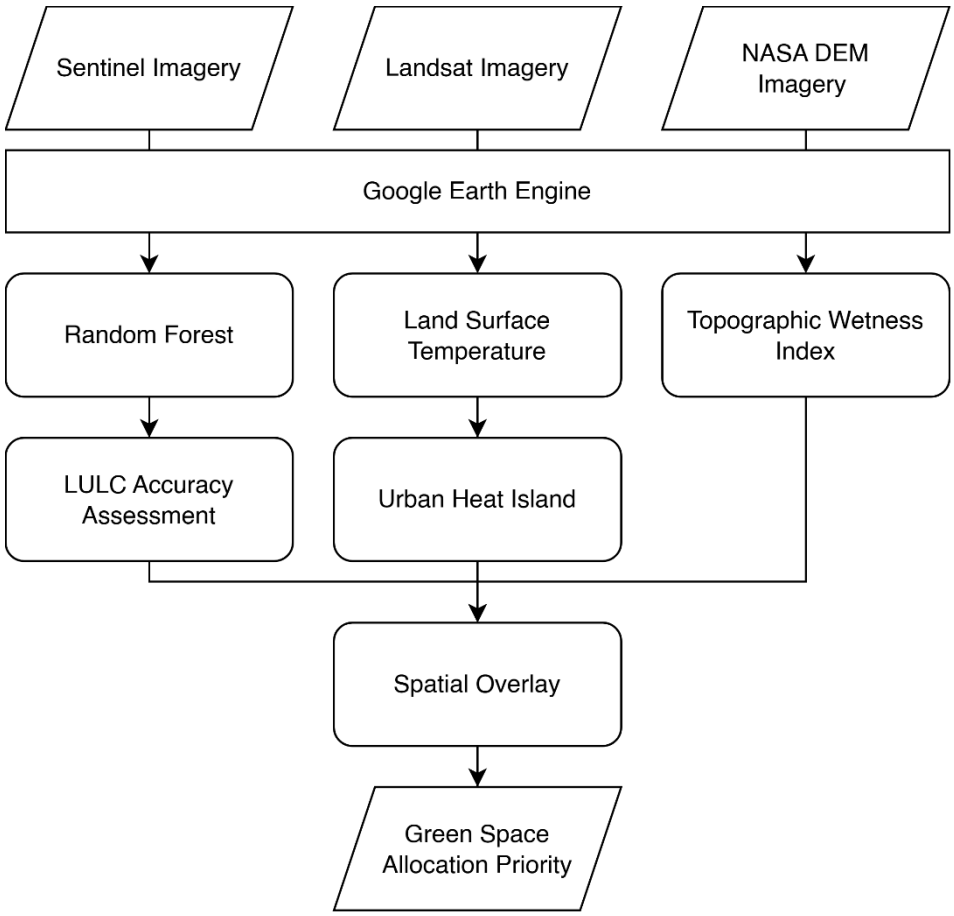


Fig. 1 Research Workflow

2.2. *Study Area*

This study was conducted in four cities in Indonesia, namely Malang, Padang, Surakarta, and Yogyakarta. These cities cover areas of approximately 111.1 km² for Malang, 694.2 km² for Padang, 46.7 km² for Surakarta, and 32.8 km² for Yogyakarta. The four cross-provincial study areas were selected based on the need to formulate a comparative urban model. The administrative maps of the four cities in the study area are presented in **Fig. 2** below. Each city represents a different spatial typology, population growth pressure, and ecological challenge, so that integrating the analysis of the four cities is expected to provide a strong basis for evaluating the effectiveness of Green Open Space (RTH) planning in responding to environmental degradation.

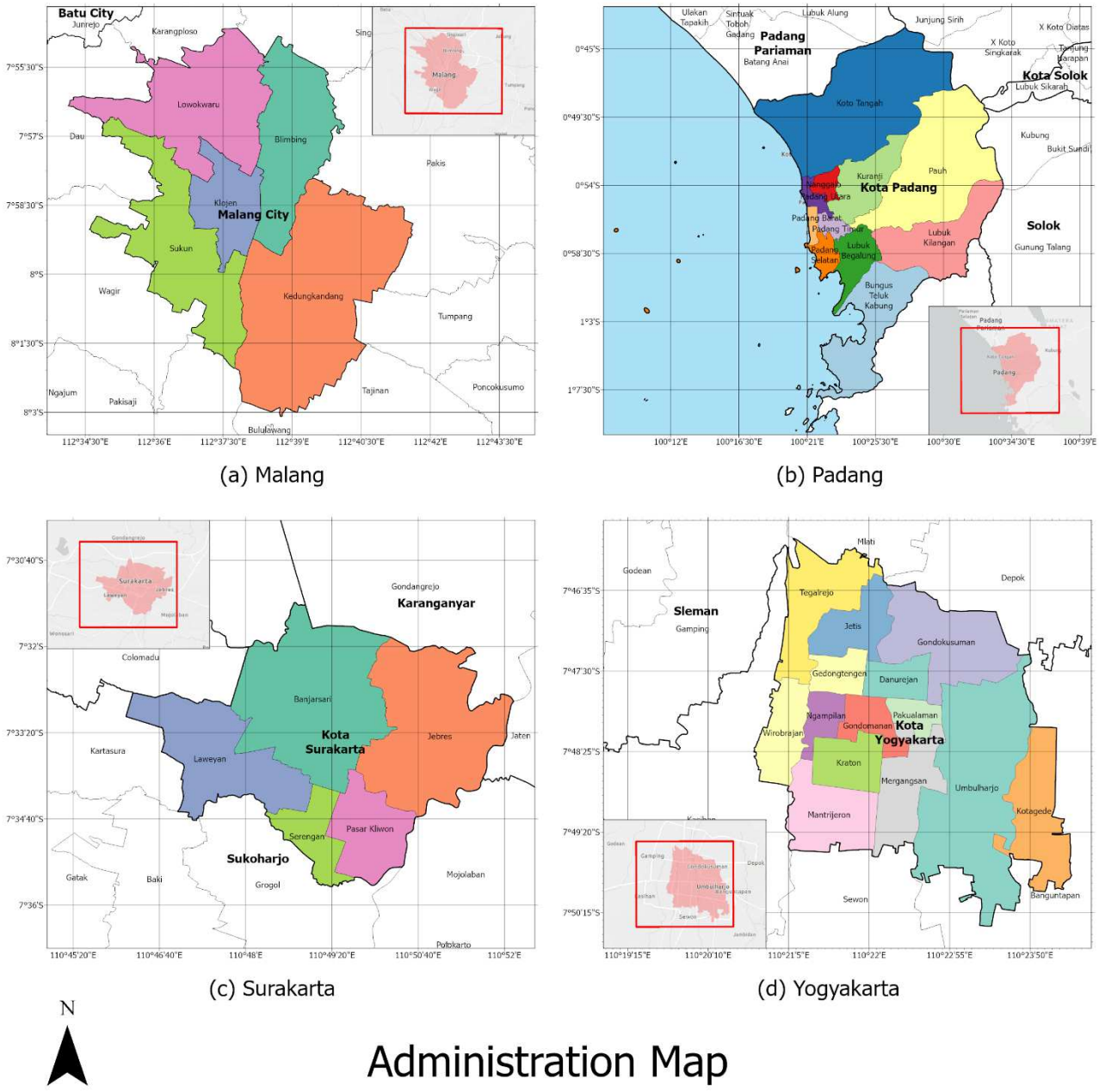


Fig. 2 Administrative Map of the Study Area. (a) Malang, (b) Padang, (c) Surakarta, (d) Yogyakarta

2.3. *Data Sources*

The initial stage of the study focused on standardizing the data architecture, beginning with data acquisition. Sentinel-2A level-2A imagery with Bottom of Atmosphere (BOA) correction was used in the Land Use and Land Cover (LULC) analysis, considering its higher spatial resolution of 10 meters. On the other hand, analyses related to surface temperature phenomena, such as Land Surface Temperature (LST) and Urban Heat Island (UHI), used Landsat 8 OLI/TIRS and Landsat 9 OLI-2/TIRS-2 level-1 imagery with Top of Atmosphere (TOA) correction. Level-1 (TOA) data were chosen because LST values in this study were calculated using mathematical equations derived directly from Brightness Temperature (BT) values in the thermal band. The acquisition dates and image types were selected based on the lowest cloud cover percentage in each study area. This criterion is also the reason two different Landsat instrument series were used. Specifically for Yogyakarta, Landsat 9 OLI-2/TIRS-2 imagery was used because this satellite recorded the area with less cloud cover during the observation

period. Meanwhile, for the Topographic Wetness Index (TWI) analysis, this study used Digital Elevation Model (DEM) data from NASA SRTM V3 imagery. Because it was recorded using radar technology (InSAR / Synthetic Aperture Radar), cloud cover does not apply to the DEM data. Further details on the satellite imagery, study areas, acquisition dates, and cloud cover percentages are presented in Table 1 below.

Table 1 Acquisition Dates and Cloud Cover of Satellite Imagery

Satellite Imagery	Study Area	Acquisition Date	Cloud Cover
Sentinel-2A	Malang City	14 August 2025	0.00 %
	Padang City	26 June 2025	1.60 %
	Surakarta City	6 June 2025	0.00 %
	Yogyakarta City	6 June 2025	0.00 %
Landsat 8 OLI/TIRS	Malang City	14 August 2025	4.70 %
	Padang City	26 June 2025	0.51 %
	Surakarta City	18 June 2025	1.06 %
Landsat 9 OLI-2/TIRS-2	Yogyakarta City	19 July 2025	0.00 %
DEM NASA SRTM V3	All study areas	11 February-22 February 2000	None

2.4. *Land Use and Land Cover Analysis*

The land cover classification stage was carried out using the Random Forest method. According to Breiman, Random Forest is an extension of CART that applies bagging and random feature selection to the Decision Tree machine learning algorithm, namely by randomly selecting several features in each iteration. The number of trees produced equals the number of iterations, resembling a forest. The classification decision is taken from the majority vote among all trees (Darmawan & Santoso, 2024; Suryono et al., 2022). Next, the classification results were validated with the help of higher-resolution imagery, namely Google satellite imagery, and their reliability was assessed through Kappa calculation. The number of points used in the validation stage was 200, with 50 points in each class. This refers to the "rule of thumb" for the number of accuracy assessment samples proposed by Russell G. Congalton. This theory explains that a minimum of 50 sample points is required for each land cover class for the validation to be considered sufficiently representative and valid (Gracia, 2021; Ridho Fariz et al., 2021). The Kappa coefficient is generally used in remote sensing to assess land cover accuracy, and is expressed in Equation 1 below (Foody, 2020; Petropoulos et al., 2015).

$$\kappa = \frac{N \sum_{i=1}^{r} x_{ii} - \sum_{i=1}^{r} (x_{i+} \cdot x_{+i})}{N^2 - \sum_{i=1}^{r} (x_{i+} \cdot x_{+i})} \qquad \text{Equation 1}$$

where: N - Total pixel observations, r - Number of land cover classes, x_{ii} - Correct samples on the main diagonal, x_{i+} - Total marginal of the i-th row, x_{+i} - Total marginal of the i-th column, Σ - Summation operation over the diagonal.

Meanwhile, the Kappa agreement table used is presented in Table 2 (Viera & Garrett, 2005).

Table 2 Kappa Agreement. Source: Viera & Garrett, 2005

Kappa Value (%)	Agreement
<0	Less than chance agreement
1-20	Slight agreement
21-40	Fair agreement
41-60	Moderate agreement
61-80	Substantial agreement
81-99	Almost perfect agreement

2.5. *Urban Heat Island Analysis*

The Urban Heat Island (UHI) value can be obtained directly through the classification of Land Surface Temperature (LST) data extracted from satellite imagery. This process begins with applying the LST algorithm to produce land surface

temperature data, derived from pixel values in the observed area. Once the surface temperature data from LST are obtained, the identification and distribution of urban heat intensity zones are evaluated using the Urban Thermal Field Variance Index (UTFVI) method. The UTFVI method specifically calculates the impact of surface temperature on environmental ecological quality, so that UHI mapping depends heavily on the accuracy of the LST algorithm as its main parameter (Abir et al., 2021; Mujahid & Irawan, 2025)

2.5.1. Land Surface Temperature

The initial step to obtain the Land Surface Temperature (LST) value is calculating brightness temperature. The conversion of spectral radiance to brightness temperature (BT) in Kelvin was performed using the equation presented in Equation 2 as follows (Stathopoulou & Cartalis, 2007).

$$BT = \frac{K_2}{\ln\left(\frac{K_1}{L_\lambda} + 1\right)} \qquad \text{Equation 2}$$

where: BT - Brightness Temperature in Kelvin, L_λ - Sensor spectral radiance (calibrated from Digital Number values), K_1 and K_2 - Thermal constants built into the satellite (for Landsat 8 Band 10, K_1 = 774.88 and K_2 = 1321.07).

The Normalized Difference Vegetation Index (NDVI) is a remote sensing calculation method used to identify the density, health, and greenness of vegetation in an area (Bannari et al., 1995). Its working principle is based on how chlorophyll in leaves responds to sunlight. Healthy plants absorb a large amount of visible light, particularly red wavelengths (Red), for use in photosynthesis. Conversely, leaves strongly reflect near-infrared (NIR) wavelengths to prevent the leaves from overheating and damaging the tissue (Mukhlisin & Soemarno, 2020). The NDVI calculation is presented in Equation 3 below.

$$NDVI = \frac{NIR - Red}{NIR + Red} \qquad \text{Equation 3}$$

where: NIR - Reflectance value of the Near-Infrared Band (Band 5 on Landsat 8), Red - Reflectance value of the Red Band (Band 4 on Landsat 8).

The Proportion of Vegetation (PV) is an estimate of the percentage of ground surface covered by the vegetation canopy (leaves, stems, branches) within a single satellite image pixel when viewed vertically from above (Carlson & Ripley, 1997). The PV calculation is presented in Equation 4 as follows (Alexander, 2020).

$$P_v = \left(\frac{NDVI - NDVI_{min}}{NDVI_{max} - NDVI_{min}}\right)^2 \qquad \text{Equation 4}$$

where: NDVI - NDVI value of the pixel being calculated, $NDVI_{min}$ - Lowest NDVI value across the study area (usually water or dense concrete areas), $NDVI_{max}$ - Highest NDVI value across the study area (usually dense forest).

Land Surface Emissivity (LSE) is a measure of how efficiently the Earth's surface emits thermal energy (thermal radiation) into the atmosphere compared with a perfect blackbody at the same temperature (Carlson & Ripley, 1997). To simplify analysis using satellite imagery (particularly Landsat), scientists have simplified the above formula into Equation 5 as follows (Sobrino et al., 2004).

$$\epsilon = 0.004 \cdot P_v + 0.986 \qquad \text{Equation 5}$$

where: The value 0.986 - the baseline emissivity of the area when it is not covered by vegetation at all (PV = 0), obtained from the combination of pure soil emissivity (0.971) plus the reflection effect of surface cavities (0.015), P_v - Proportion of Vegetation, with the boundary conditions of the Sobrino formula setting an emissivity value of 0.971 for bare soil ($P_v = 0$), 0.990 for full vegetation ($P_v = 1$), and 0.995 for water bodies, The value 0.004 - the difference between full-vegetation emissivity (0.990) and the baseline emissivity above (0.986), which indicates how much emissivity increases each time the vegetation proportion increases.

Land Surface Temperature (LST) is a measure of the actual temperature of the Earth's surface when directly exposed to solar radiation. It differs from the daily air temperature (ambient temperature) commonly seen in weather applications,

because LST measures how hot materials on the Earth's surface (such as asphalt, tree canopy, or soil) radiate energy back into the atmosphere (Avdan & Jovanovska, 2016). The LST calculation is presented in Equation 6 as follows.

$$LST = \frac{BT}{1 + \left(\frac{\lambda \cdot BT}{\rho}\right) \ln(\epsilon)} - 273.15 \qquad \text{Equation 6}$$

where: BT - Brightness Temperature, λ - Emitted wavelength of the satellite thermal sensor used, ρ - Thermodynamic constant with a value of 14380 (this value is obtained from ρ = h × c / σ, where h is Planck's constant, c is the speed of light, and σ is the Boltzmann constant), LSE - Land Surface Emissivity calculated from the Proportion of Vegetation (PV), The value - 273.15 – is the subtraction value used to convert temperature from Kelvin to Celsius.

2.5.2. Urban Heat Island

As the final stage of the analysis, the presence of the Urban Heat Island (UHI) was evaluated using the Urban Thermal Field Variance Index (UTFVI) parameter (Abir et al., 2021). This parameter is used because of its specific capability to quantify the impact of surface temperature on environmental ecological quality. This classification mapping visualizes the spatial distribution of heat intensity to identify areas with high thermal risk. The UHI calculation is presented in Equation 7 as follows. Based on the Ecological Evaluation Index (EEI), UTFVI values are classified into six categories, from the best to the worst, as shown in Table 3. These six categories were then reclassified into two priority classes to determine which areas have low or high priority in future RTH allocation planning.

$$UTFVI = \frac{T_s - T_{mean}}{T_{mean}} \qquad \text{Equation 7}$$

where: T_s - LST value at a given point/pixel, T_{mean} - Mean LST value of the entire study area.

Table 3 UTFVI Value Ranges. Source: Abir et al., 2021

UTFVI	UHI Presence	Priority
< 0	None	
0.000 - 0.005	Weak	Low
0.005 - 0.010	Moderate	
0.010 - 0.015	Strong	
0.015 - 0.020	Very Strong	High
> 0.020	Extreme	

2.6. *Topographic Wetness Index Analysis*

The Topographic Wetness Index (TWI) was first developed by Beven and Kirkby (1979) as part of runoff modeling. TWI assesses the effect of local topography on the resulting runoff (Pourali et al., 2016). TWI is an index used in hydrological analysis to describe the tendency of an area to accumulate water. TWI is a method that can be used for rapid flood assessment, using Digital Elevation Model (DEM) data, and also for more detailed flood modeling (Paiman & Purwanto, 2025). To extract the flow accumulation variable, this study used the flow tracing algorithm of the MERIT Hydro dataset. MERIT Hydro is a high-resolution global hydrography map that carefully maps surface flow directions using an algorithm that separates genuine inland basins from artificial depressions caused by errors in elevation data (Yamazaki et al., 2019). The main formula used in the TWI calculation is presented in Equation 8 as follows (Beven & Kirkby, 1979).

$$W = \ln\left(\frac{a}{\tan\beta}\right) \qquad \text{Equation 8}$$

where: W - Wetness index value (TWI), a - Upslope accumulation (upslope contributing area or specific catchment area) that drains water to a point per unit contour, β (or tan β) - Slope angle at that point, which in practice is converted into its tangent after being converted to radians.

To make the interpretation of spatial data easier, the Topographic Wetness Index (TWI) data were normalized, a step that simplifies and standardizes data analysis by transforming the actual range of values into a defined interval, namely

between 0 and 1. Values close to 1 represent lowland areas with high potential for water accumulation or inundation, whereas values close to 0 represent drier hilly or mountainous areas. The equation used to obtain the normalized values is presented in Equation 9 below (Nucifera & Putro, 2017).

$$Normalized\ TWI = \frac{a + (x - A)(b - a)}{(B - A)} \qquad \text{Equation 9}$$

where: x - Actual TWI value at the point or pixel to be normalized, A and B - Respectively the lowest and highest actual TWI values found across the entire study area, a and b - Desired normalization range limit parameters, where a is set as the lowest normalization limit, namely 0, and b is set as the highest normalization limit, namely 1, to produce a dimensionally uniform index between 0 and 1 through proportional adjustment to the difference between the maximum and minimum values of the area.

Next, to determine high-priority areas for RTH allocation, the calculated TWI values were classified into two classes using the mean value as the threshold. Using this method, areas with TWI values above the mean were categorized as zones with high runoff potential, while areas with values below it were classified as low-runoff zones.

3. Results and Discussion

3.1. *Land Use and Land Cover Analysis*

Based on the land cover classification results using Sentinel-2 imagery with the Random Forest algorithm, a high classification accuracy was obtained, with Overall Accuracy values ranging from 92.50% to 94.50% and Kappa Coefficient values ranging from 90% to 93%. These confusion matrix results indicate an almost perfect agreement level based on the Kappa statistic for all study areas. The classification used a value of 50 for the Number of trees parameter to produce a stable and precise model without triggering the risk of overfitting. In more detail, the Kappa calculation for each study area is presented in Table 4 below.

Table 4 LULC Accuracy Assessment Calculation

Study Area	Land Cover	Built-up	Barren land	Vegetation	Water body	Total	U_Accuracy (%)	Kappa (%)
Malang City	**Built-up**	49	1	0	0	50	98	
	Barren land	0	50	0	0	50	100	
	Vegetation	9	0	41	0	50	82	
	Water body	0	0	1	49	50	98	
	Total	58	51	42	49	200	0	
	P_Accuracy (%)	84	98	98	100	0	95	
	Kappa (%)							**93**
Padang City	**Built-up**	44	5	1	0	50	88	
	Barren land	3	46	1	0	50	92	
	Vegetation	2	2	46	0	50	92	
	Water body	0	1	0	49	50	98	
	Total	49	54	48	49	200	0	
	P_Accuracy (%)	90	85	96	100	0	93	
	Kappa (%)							**90**
Surakarta City	**Built-up**	47	0	3	0	50	94	
	Barren land	6	44	0	0	50	88	
	Vegetation	1	0	49	0	50	98	
	Water body	0	0	1	49	50	98	
	Total	54	44	53	49	200	0	
	P_Accuracy (%)	87	100	92	100	0	95	

Study Area	Land Cover	Built-up	Barren land	Vegetation	Water body	Total	U_Accuracy (%)	Kappa (%)
	Kappa (%)							93
Yogyakarta City	**Built-up**	50	0	0	0	50	100	
	Barren land	0	50	0	0	50	100	
	Vegetation	13	0	37	0	50	74	
	Water body	1	0	0	49	50	98	
	Total	64	50	37	49	200	0	
	P_Accuracy (%)	78	100	100	100	0	93	
	Kappa (%)							**91**

The reliability of the model is evidenced by the high Producer Accuracy (representing the minimum omission error), which reached a perfect value (100%) for the Barren land and Water body classes, indicating the algorithm's success in mapping actual field conditions. In line with this, the User Accuracy (representing the minimum commission error) also shows a very good level of agreement between the map and reality overall.

Table 5 Land Cover Area

Land Cover	Area (km²)			
	Malang	**Padang**	**Surakarta**	**Yogyakarta**
Built-up	54.64	95.29	38.63	27.48
Barren land	0.48	4.59	0.32	0.13
Vegetation	55.92	591.88	7.33	5.13
Water body	0.03	2.46	0.41	0.04

The calculation and distribution of land cover areas in Table 5 and **Fig. 3** show highly contrasting spatial characteristics among the cities. Padang has a very dominant Vegetation area of 591.88 km², far exceeding the other land cover classes. In contrast, Surakarta and Yogyakarta show signs of high urbanization pressure, marked by the dominance of the Built-up class at 38.63 km² and 27.48 km², respectively, in sharp contrast to the minimal presence of Vegetation (7.33 km² and 5.13 km²). Meanwhile, Malang shows a relatively balanced spatial composition between Built-up (54.64 km²) and Vegetation (55.92 km²). The proportions of Barren land and Water body in the four urban areas are not dominant land cover components.

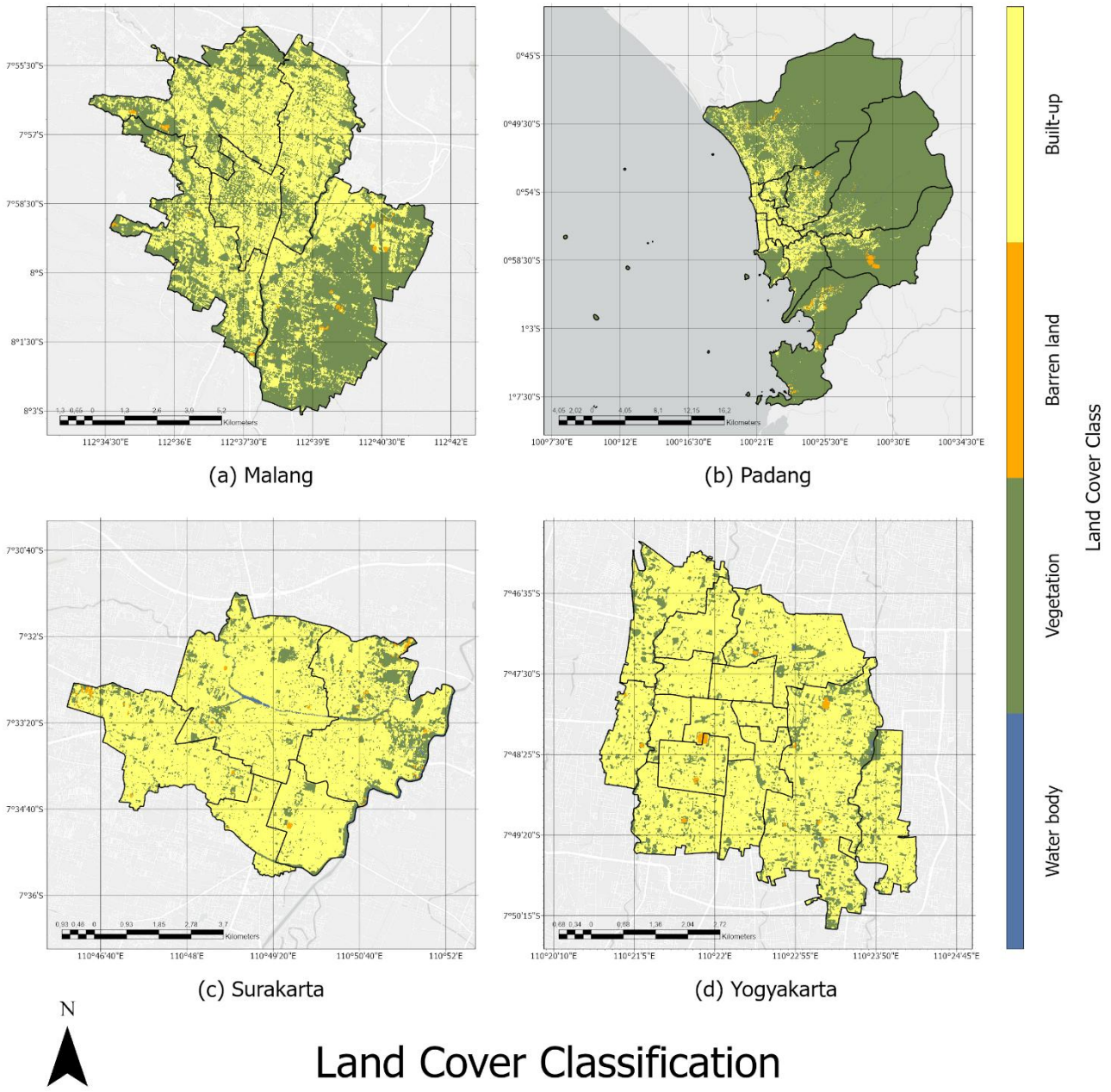


Fig. 3 Land Cover Classification Map. (a) Malang, (b) Padang, (c) Surakarta, (d) Yogyakarta

3.2. *Urban Heat Island Analysis*

The distribution of Land Surface Temperature (LST) in the four study cities, namely Padang, Yogyakarta, Surakarta, and Malang, is presented in **Fig. 4**. The imagery used consists of Landsat scenes recorded at different times according to the availability of cloud-free images, all within the morning time range of 09.00-11.00, so that the LST values obtained represent the surface temperature conditions of each city at the time of recording. Selecting imagery with the lowest possible cloud cover is very important to avoid atmospheric interference that can reduce the accuracy of thermal value extraction. Visually, the spatial distribution pattern of surface temperature generally shows a consistent correlation with land cover characteristics, in which the highest temperature clusters tend to accumulate in Built-up areas.

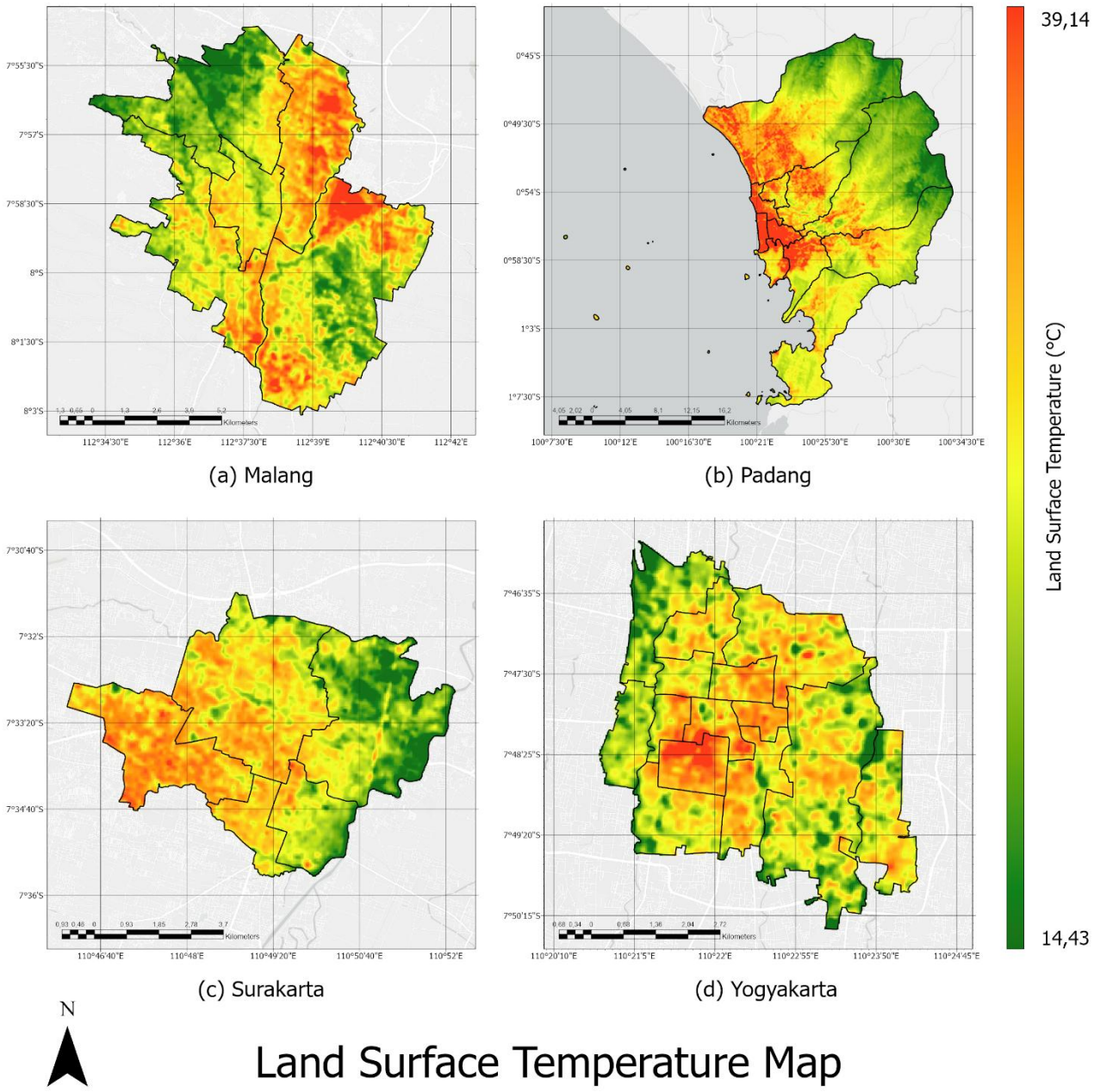


Fig. 4 Land Surface Temperature Map. (a) Malang, (b) Padang, (c) Surakarta, (d) Yogyakarta

The calculated land surface temperature (Land Surface Temperature/LST) values in the four study areas show differences in spatial thermal characteristics, as shown in **Fig. 5**. Yogyakarta recorded the highest surface temperature intensity, with a maximum of 39.14 °C and a minimum of 26.47 °C. In contrast, Padang showed the widest thermal range, marked by the lowest minimum temperature of all study areas, 14.43 °C, but also a relatively high maximum temperature of 32.26 °C. Meanwhile, the surface temperature distribution in Malang lies within a more moderate range, from 18.98 °C to 31.37 °C. On the other hand, Surakarta shows the narrowest thermal range, with the lowest maximum temperature among the four cities at 27.55 °C and a minimum temperature limit of 19.40 °C.

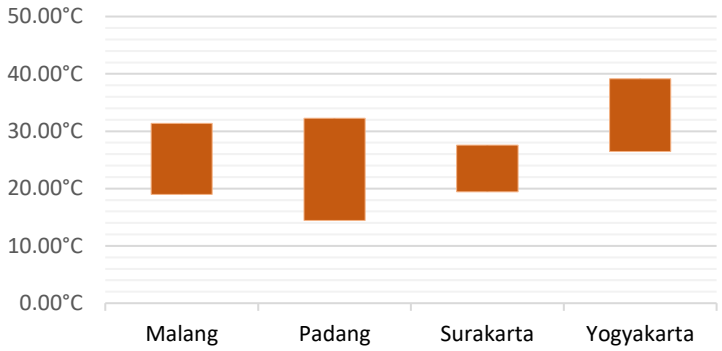


Fig. 5 LST Value Range Chart

Next, the mean Land Surface Temperature (LST) of each study city and the Urban Thermal Field Variance Index (UTFVI) areas obtained are presented in Table 6. The city-scale mean LST calculation shows variation in thermal conditions across the study areas. Yogyakarta recorded the highest mean surface temperature intensity, reaching 31.56 °C. In contrast, Padang recorded the lowest mean LST at 22.71 °C. Meanwhile, Malang and Surakarta show moderate and closely similar mean surface temperature profiles, at 25.07 °C and 24.47 °C, respectively.

Table 6 Mean LST and UTFVI Area

City	Mean LST (°C)	UTFVI Area (km²)					
		None	Weak	Moderate	Strong	Very Strong	Extreme
Malang	25.07	54.14	2.82	2.91	3.05	2.99	44.97
Padang	22.71	369.75	13.02	13.66	13.08	11.81	272.32
Surakarta	24.47	20.58	1.73	1.83	1.92	1.83	18.83
Yogyakarta	31.56	15.27	2.50	2.42	2.36	2.19	7.89

Based on the distribution of Urban Thermal Field Variance Index (UTFVI) areas, the values in the four cities show a very clear spatial pattern. The UTFVI area profile in each city is dominated by two opposing categories, namely the "None" and "Extreme" categories. This is seen in all areas, such as Padang with a "None" area of 369.75 km² and an "Extreme" area of 272.32 km², as well as Malang with 54.14 km² and 44.97 km² in the two categories. The same dominance pattern also occurs in Surakarta, where the "None" category covers 20.58 km² and the "Extreme" category reaches 18.83 km², and in Yogyakarta, with distributions of 15.27 km² and 7.89 km², respectively, for the two categories. In contrast, the spatial extent of areas with intermediate or transitional vulnerability, namely the weak, moderate, strong, and very strong ranges, accounts for a very minimal proportion in the four urban areas.

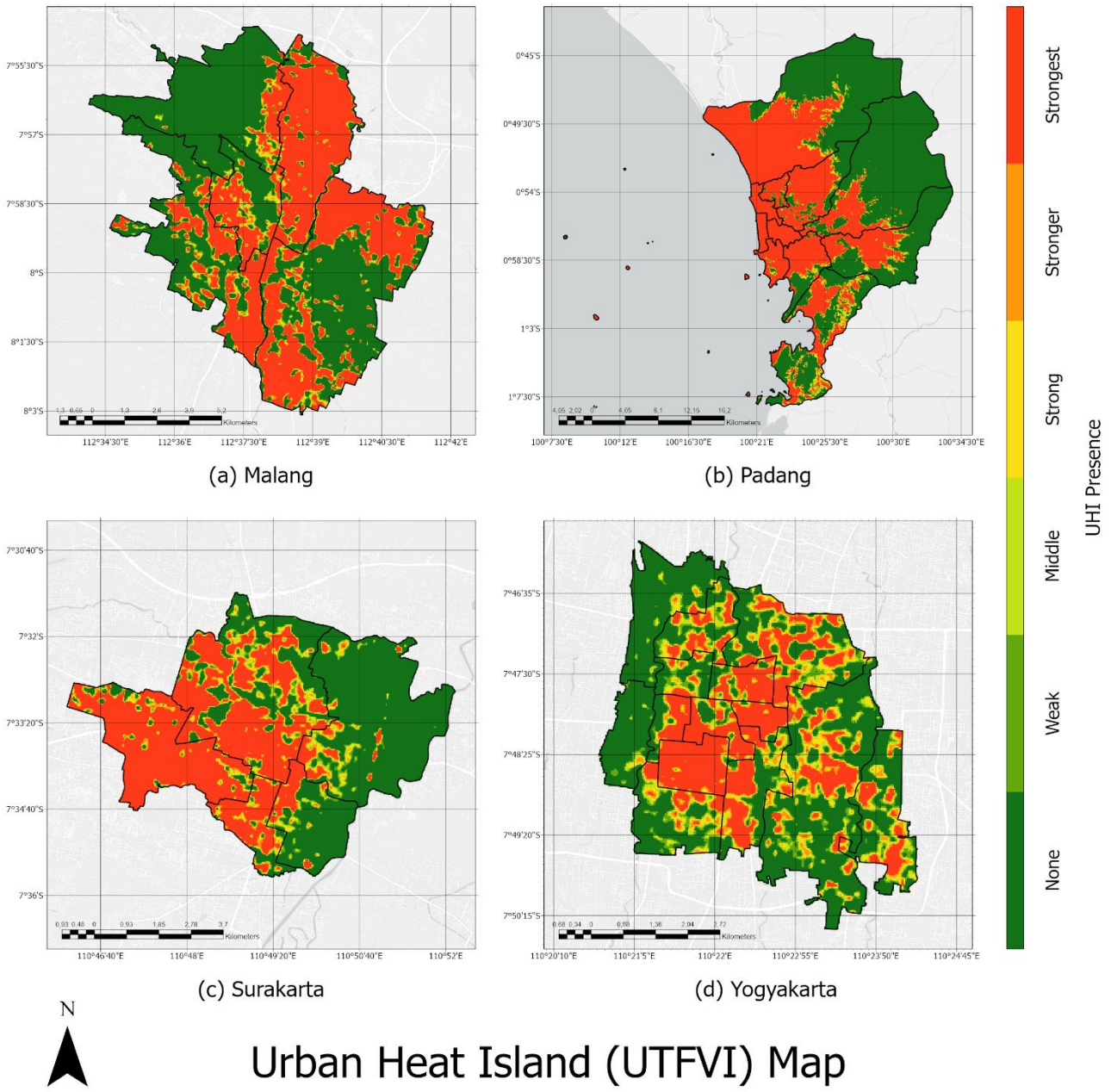


Fig. 6 Urban Heat Island (UTFVI) Map. (a) Malang, (b) Padang, (c) Surakarta, (d) Yogyakarta

3.3. *Topographic Wetness Index Analysis*

The Topographic Wetness Index (TWI) analysis using Digital Elevation Model (DEM) data from SRTM V3 at 30 m spatial resolution shows that the study areas are still dominated by the low TWI class (< mean), with proportions ranging from 61% to 68%, as presented in **Fig. 7** and **Fig. 8**. Padang recorded the largest area of high TWI (> mean), or areas with inundation potential, at 38.05%. Meanwhile, Malang, Yogyakarta, and Surakarta show a relatively uniform distribution of areas with inundation potential, recorded at 32.31%, 31.61%, and 31.31%, respectively. Overall, more than 30% of the spatial area in the four cities was identified as naturally vulnerable to surface water accumulation.

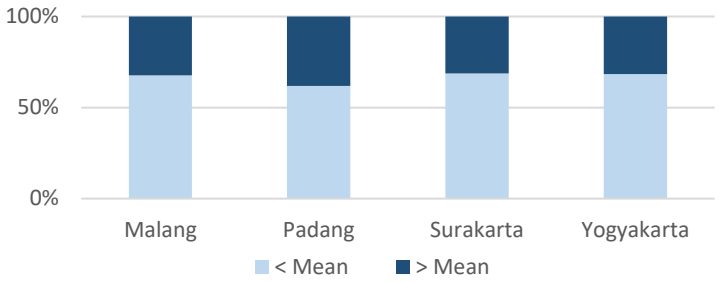


Fig. 7 TWI Value Range Chart

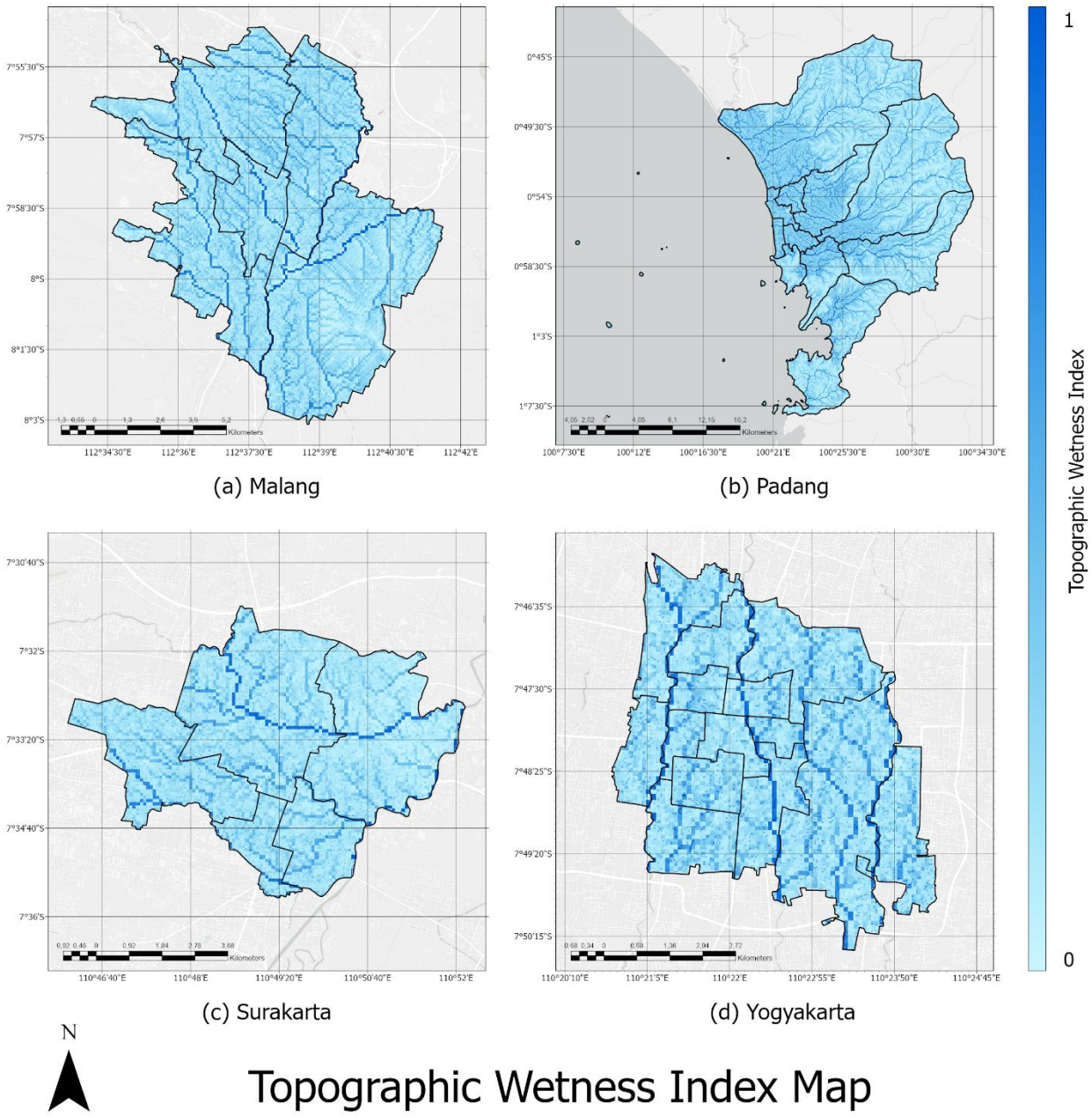


Fig. 8 Topographic Wetness Index Map. (a) Malang, (b) Padang, (c) Surakarta, (d) Yogyakarta

3.4. *Synchronization of LULC, UHI, and TWI*

Previous studies have integrated various geospatial variables to map environmental vulnerability and urban thermal dynamics. For example, Papakonstantinou (2025) used a combination of satellite-derived indices, including land surface temperature (LST) and topographic wetness index (TWI), to identify extreme heat and moisture vulnerability zones for vulnerable urban populations. A similar approach was also implemented by Aslan and Koc-San (2021), who demonstrated the effectiveness of using land cover indices from multi-temporal satellite imagery to detect surface urban heat island (SUHI) phenomena quickly and efficiently. The integration of such biophysical parameters, including land use and land cover (LULC) and topography, has been shown to have a significant nonlinear relationship with LST fluctuations, in which land cover characteristics play a dominant role in thermal conditions.

The application of these geospatial and thermal parameters has been widely adopted in building spatial planning frameworks to prioritize the development of urban green infrastructure (UGI) or green open space (RTH). Norton et al. (2015) developed a priority framework to identify high-risk urban neighborhoods by integrating heat exposure and vulnerability data to maximize the surface cooling benefits of green infrastructure. In a related context, Meerow and Newell (2017) introduced a multi-criteria spatial planning model that integrates urban heat island (UHI) mitigation with stormwater management and social factors to strategically identify priority locations (hotspots) for green infrastructure expansion. Whereas these earlier studies generally focus on broad ecosystem services or demographic vulnerability metrics, the present study specifically overlays LULC, UHI, and TWI to produce a spatial approach more focused on the physical environmental parameters in determining RTH development priority allocation, in line with recent spatial modeling confirming that vegetation cover and high surface water content have a significant impact on reducing the UHI effect (Gidey & Mhangara, 2025).

The spatial synchronization among Land Use and Land Cover (LULC), Urban Heat Island (UHI) based on the UTFVI index, and Topographic Wetness Index (TWI) is intended as a basis for preparing a policy brief and recommendations in spatial planning documents regarding the allocation of Green Open Space (RTH). This synchronization begins by simplifying the UTFVI classification from the original six classes into two categories, namely high priority, covering the top three classes with maximum thermal exposure, and low priority for the bottom three classes. Meanwhile, the TWI classification uses an adaptive threshold approach, in which areas with values above the mean in each study city are designated as high priority, while values below the mean are categorized as low priority. The overlay of these two categorizations produces the priority matrix presented in Table 7.

Table 7 Priority Matrix

UHI Classification	TWI Classification	Priority
High	High	I
	Low	II
Low	High	III
	Low	IV

To produce precise intervention directives, the priority map was integrated with Land Use and Land Cover (LULC) data. This overlay process maps the distribution of Priority Scenario I (Dual-Risk Zone: High Heat and High Inundation Potential) across the Built-up, Barren land, and Vegetation classes to determine the most relevant form of RTH adaptation for existing conditions. Specifically, where a Priority Scenario I zone coincides with Water body land cover, the area is not recommended for conversion, but is instead conserved and retained for its designated use to ensure the sustainability of its natural hydrological functions.

Table 8 Area of RTH Allocation Priority Classes

City	Priority Class (km²)			
	Non-Priority	High Priority: Built-up	High Priority: Barren land	High Priority: Vegetation
Malang	94.68	10.39	0.05	5.96
Padang	527.74	67.33	2.29	96.84
Surakarta	38.97	7.09	0.03	0.59
Yogyakarta	28.93	3.56	0.03	0.27

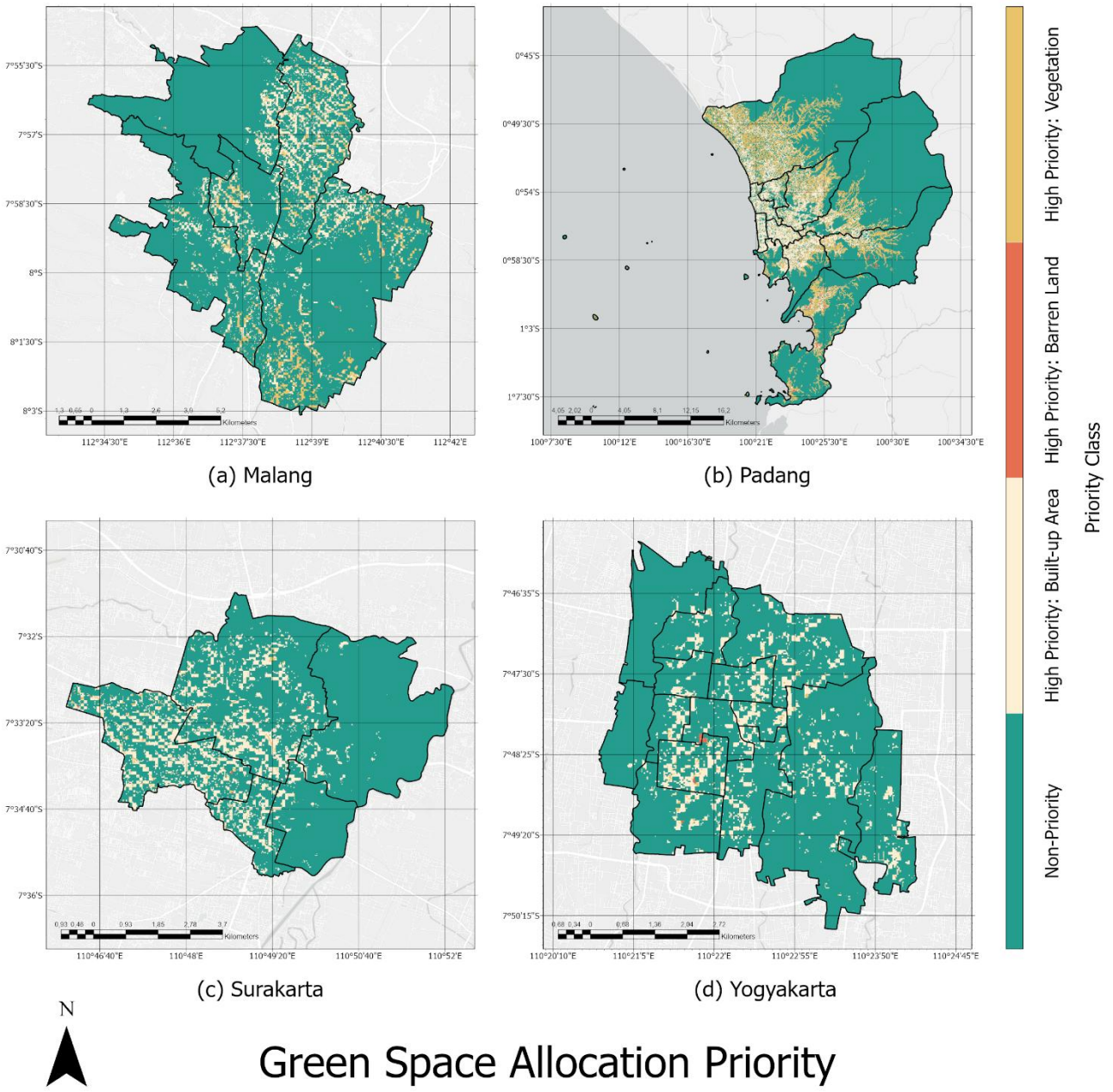


Fig. 9 RTH Allocation Priority Map. (a) Malang, (b) Padang, (c) Surakarta, (d) Yogyakarta

Based on the spatial analysis presented in Table 8, the distribution of Priority Scenario I areas (Dual-Risk Zone: High Heat and High Inundation Potential) shows different land cover characteristics among the study areas. In the urban areas on Java Island, namely Malang, Surakarta, and Yogyakarta, Priority Scenario I is consistently dominated by the Built-up class, with areas of 10.39 km², 7.09 km², and 3.56 km², respectively. In contrast, in Padang, the Priority Scenario I area is dominated by the Vegetation class, reaching 96.84 km², followed by Built-up at 67.33 km². Given the large Built-up area included in Priority Scenario I across all study cities, and the fact that redevelopment or eviction in densely built areas is unrealistic from a spatial planning perspective, the policy direction for this class can focus on micro-scale interventions. These interventions include implementing green roofs, vertical gardens, permeable pavement materials, and constructing infiltration wells.

On the other hand, Priority Scenario I areas located on existing Vegetation land cover play a very crucial role, particularly in Padang, where they are overwhelmingly dominant (96.84 km²), as well as in Malang (5.96 km²). Vegetation in this zone bears the main ecological burden of reducing the Urban Heat Island (UHI) and naturally retaining the area's water

accumulation. Therefore, the recommended policy intervention is to impose a conservation or strict protection status. The government must integrate this protection into zoning regulations to prohibit all forms of land conversion permits from Vegetation to Built-up. Meanwhile, the availability of Barren land in the Priority Scenario I areas is very limited across the four study areas (ranging only from 0.03 km² to 2.29 km²). Local governments are recommended to promptly acquire the remaining Barren land, because these locations are the most ideal points for building new Green Open Space (RTH) that can absorb heat and runoff optimally.

4. Conclusion

The land cover classification results using the Random Forest algorithm show varying spatial proportions, in which Yogyakarta and Surakarta are dominated by Built-up, at 83.83% (27.48 km²) and 82.74% (38.63 km²), respectively, while Padang and Malang retain dominant Vegetation, at 85.26% (591.88 km²) and 50.35% (55.92 km²). Based on the calculations, the highest city-scale mean Land Surface Temperature (LST) was recorded in Yogyakarta at 31.56 °C, followed by Malang at 25.07 °C and Surakarta at 24.47 °C, while Padang recorded the lowest mean at 22.71 °C due to the strong influence of its mountainous areas and geographic location. Despite these mean results, Urban Heat Island (UHI) mapping specifically found that the largest area exposed to extreme temperature anomalies was in Padang, at 272.32 km², in sharp contrast with the high-temperature-prone areas in Malang (44.97 km²), Surakarta (18.83 km²), and Yogyakarta (7.89 km²). The hydrological vulnerability assessment using the Topographic Wetness Index (TWI) with the mean value as the threshold shows that the study areas are generally dominated by the low TWI class (< mean), with proportions of 61% to 68%, while the high TWI class (> mean), which has the potential for surface runoff accumulation or inundation, accounts for the largest proportion in Padang (38.05%), followed by Malang (32.31%), Yogyakarta (31.61%), and Surakarta (31.31%).

The spatial synchronization of LULC, UHI, and TWI in the four study cities produces an RTH allocation priority matrix dominated by the non-priority class, with the highest proportion in Yogyakarta (88.22% of 32.8 km²) and the lowest in Padang (76.02% of 694.2 km²), indicating that only a small part of each area has an overlap between extreme heat exposure and high inundation potential. In Priority Scenario I (Dual-Risk Zone: High Heat and High Inundation Potential), the cities on Java Island (Malang, Surakarta, and Yogyakarta) are dominated by the Built-up class, whereas Padang is dominated by the Vegetation class followed by Built-up. For Built-up in this zone, the recommended policy direction is micro-scale intervention such as green roofs and infiltration wells. Barren land in Priority Scenario I is very limited (0.05%-0.33%) and should therefore be promptly acquired for new RTH, while existing Vegetation that bears a heavy ecosystem burden in this zone, especially in Padang (13.95%) and Malang (5.37%), must be maintained through strict zoning protection policies.

5. References

Abir, F. A., Ahmmed, S., Sarker, S. H., & Fahim, A. U. (2021). Thermal and ecological assessment based on land surface temperature and quantifying multivariate controlling factors in Bogura, Bangladesh. *Heliyon*, *7*(9). https://doi.org/10.1016/j.heliyon.2021.e08012

Alexander, C. (2020). Normalised difference spectral indices and urban land cover as indicators of land surface temperature (LST). *International Journal of Applied Earth Observation and Geoinformation*, *86*, 102013. https://doi.org/10.1016/j.jag.2019.102013

Aslan, N., & Koc-San, D. (2021). The Use of Land Cover Indices for Rapid Surface Urban Heat Island Detection from Multi-Temporal Landsat Imageries. In *ISPRS International Journal of Geo-Information* (Vol. 10, Issue 6, p. 416). https://doi.org/10.3390/ijgi10060416

Avdan, U., & Jovanovska, G. (2016). Algorithm for Automated Mapping of Land Surface Temperature Using LANDSAT 8 Satellite Data. *Journal of Sensors*, *2016*(1), 1480307. https://doi.org/10.1155/2016/1480307

Bannari, A., Morin, D., Bonn, F., & Huete, A. R. (1995). A review of vegetation indices for vegetation monitoring. *Remote Sensing Reviews*, *13*(1–2), 95–120. https://doi.org/10.1080/02757259509532298

Beven, K. J., & Kirkby, M. J. (1979). A physically based, variable contributing area model of basin hydrology / Un modèle à base physique de zone d'appel variable de l'hydrologie du bassin versant. *Hydrological Sciences Bulletin*, *24*(1), 43–69. https://doi.org/10.1080/02626667909491834

Carlson, T. N., & Ripley, D. A. (1997). On the relation between NDVI, fractional vegetation cover, and leaf area index. *Remote Sensing of Environment*, *62*(3), 241–252. https://doi.org/10.1016/S0034-4257(97)00104-1

Darmawan, A., & Santoso, T. (2024). Mapping Urban Transformation: The Random Forest Algorithm to Monitor Land Use and Land Cover Change in Bandar Lampung City. *Jurnal Sylva Lestari*, *12*(3 SE-Articles), 980–997. https://doi.org/10.23960/jsl.v12i3.960

Fadhillah, R. R. (2025). *Analisis Kesesuaian Penggunaan Tanah Terhadap Rencana Detail Tata Ruang dan Prediksi Kesesuaian Penggunaan Tanah (Studi di Kota Yogyakarta, Provinsi Daerah Istimewa Yogyakarta)* [Sekolah Tinggi Pertanahan Nasional]. http://repository.stpn.ac.id/id/eprint/4532

Foody, G. M. (2020). Explaining the unsuitability of the kappa coefficient in the assessment and comparison of the accuracy of thematic maps obtained by image classification. *Remote Sensing of Environment*, *239*, 111630. https://doi.org/10.1016/j.rse.2019.111630

Gidey, E., & Mhangara, P. (2025). Improving spatial modeling framework to assess the impact of vegetation cover , water content , and surface temperature on urban heat island effects in Johannesburg , South Africa. *Discover Environment*. https://doi.org/10.1007/s44274-025-00264-0

Gracia, E. (2021). *Pemanfaatan Citra Landsat 8 Untuk Identifikasi Perkembangan Vegetasi di Kabupaten Gowa Tahun 2015 Dan Tahun 2020*. https://doi.org/10.13140/RG.2.2.18601.72803

Güneralp, B., Reba, M., Hales, B. U., Wentz, E. A., & Seto, K. C. (2020). Trends in urban land expansion, density, and land transitions from 1970 to 2010: a global synthesis. *Environmental Research Letters*, *15*(4), 44015. https://doi.org/10.1088/1748-9326/ab6669

Hannum, K., Wellstead, A. M., Howlett, M., & Gofen, A. (2025). Leveraging GIS for policy design: spatial analytics as a strategic tool. *Policy Design and Practice*, *8*(1), 35–49. https://doi.org/10.1080/25741292.2025.2474784

Hasyim, A., Rini Dwi Ari, I., Setyono, D., Nugroho, A., & Christiawan, B. (2024). Growth Characteristics of Malang City Based on Sentinel 2A Multitemporal Imagery Data. *Evergreen*, *11*, 1201–1209. https://doi.org/10.5109/7183424

Hasyim, A., Sukojo, B., Fatahillah, E., Anggraini, I., & Isdianto, A. (2025). Assessing the Impact of Population Density and Land Use on Land Surface Temperature for Sustainable Urban Planning in Malang City, Indonesia. *International Journal of Sustainable Development and Planning*, *20*, 2179–2191. https://doi.org/10.18280/ijsdp.200533

Isdianto, A., Hasyim, A. W., Sukojo, B. M., & Alimuddin, I. (2025). *International Journal of Sustainable Development and Planning Integrating Urban Design with Natural Dynamics : Enhancing Ecological Resilience in Malang City over a Decade*. *20*(3), 1061–1075.

Jatayu, A., & Susetyo, C. (2018). Analisis Perubahan Temperatur Permukaan Wilayah Surabaya Timur Tahun 2001-2016 Menggunakan Citra LANDSAT. *Jurnal Teknik ITS*, *6*. https://doi.org/10.12962/j23373539.v6i2.24504

Liu, X., Huang, Y., Xu, X., Li, X., Li, X., Ciais, P., Lin, P., Gong, K., Ziegler, A. D., Chen, A., Gong, P., Chen, J., Hu, G., Chen, Y., Wang, S., Wu, Q., Huang, K., Estes, L., & Zeng, Z. (2020). High-spatiotemporal-resolution mapping of global urban change from 1985 to 2015. *Nature Sustainability*, *3*(7), 564–570. https://doi.org/10.1038/s41893-020-0521-x

Meerow, S., & Newell, J. P. (2017). Landscape and Urban Planning Spatial planning for multifunctional green infrastructure : Growing resilience in Detroit. *Landscape and Urban Planning*, *159*, 62–75. https://doi.org/10.1016/j.landurbplan.2016.10.005

Mujahid, H. I., & Irawan, L. Y. (2025). Identifikasi Urban Heat Island (UHI) Melalui Teknologi Penginderaan Jauh di Provinsi DKI Jakarta Tahun 2023. *JTSL (Jurnal Tanah Dan Sumberdaya Lahan)*, *12*(1 SE-Articles), 117–126. https://doi.org/10.21776/ub.jtsl.2025.012.1.12

Mukhlisin, A., & Soemarno, S. (2020). Estimasi Kandungan Klorofil Tanaman Kopi Robusta (Coffea canephora var. Robusta) Menggunakan Normalized Difference Vegetation Index (Ndvi) di Bangelan, Wonosari, Malang. *JTSL (Jurnal Tanah Dan Sumberdaya Lahan)*, *7*(2 SE-Articles), 329–339. https://doi.org/10.21776/ub.jtsl.2020.007.2.18

Norton, B. A., Coutts, A. M., Livesley, S. J., Harris, R. J., Hunter, A. M., & Williams, N. S. G. (2015). Landscape and Urban Planning Planning for cooler cities : A framework to prioritise green infrastructure to mitigate high temperatures in urban landscapes. *Landscape and Urban Planning*, *134*, 127–138. https://doi.org/10.1016/j.landurbplan.2014.10.018

Nucifera, F., & Putro, S. T. (2017). Deteksi Kerawanan Banjir Genangan Menggunakan Topographic Wetness Index (TWI). *Media Komunikasi Geografi*, *Vol. 18 No. 2 (2017)*, 107–116. https://ejournal.undiksha.ac.id/index.php/MKG/article/view/12088/8201

Paiman, P., & Purwanto, A. (2025). Analisis Banjir di Sungai Ambawang Menggunakan Topography Wetness Index. *J SIG (Jurnal Sains Informasi Geografi)*, *8*(2), 60–69. https://doi.org/10.31314/jsig.v8i2.4602

Papakonstantinou, G. F. D. (2025). Identifying Extreme Heat and Moisture Zones for Vulnerable Populations in Athens: A Geospatial Analysis. In *Land* (Vol. 14, Issue 7, p. 1375). https://doi.org/10.3390/land14071375

Petropoulos, G. P., Kalivas, D. P., Georgopoulou, I. A., & Srivastava, P. K. (2015). Urban vegetation cover extraction from hyperspectral imagery and geographic information system spatial analysis techniques: case of Athens, Greece. *Journal of Applied Remote Sensing*, *9*(1), 96088. https://doi.org/10.1117/1.JRS.9.096088

Pourali, S., Arrowsmith, C., Chrisman, N., Matkan, A., & Mitchell, D. (2016). *Topography Wetness Index Application in Flood-Risk-Based Land Use Planning*. https://research-repository.rmit.edu.au/articles/journal_contribution/Topography_Wetness_Index_Application_in_Flood-Risk-Based_Land_Use_Planning/27474900

Ramdhan, M. (2021). *Metode Penelitian*. Cipta Media Nusantara. https://books.google.co.id/books?id=Ntw_EAAAQBAJ

Ratnasari, A., Sitorus, S. R. P., & Tjahjono, B. (2015). Perencanaan kota hijau Yogyakarta berdasarkan penggunaan lahan dan kecukupan RTH. *TATALOKA*, *17*(4), 196–208. https://doi.org/10.14710/tataloka.17.4.196-208

Refnitasari, L., Wiyono, A., Kamila, N. P., Makhmudiyah, N., Amudi, A., Soeparno, S., & Pattisinai, A. R. (2025). Analysis of Urban Land Use Changes in Surabaya for The Years 2019-2024 Through Geographic Information System Processing. *E3S Web Conf.*, *645*. https://doi.org/10.1051/e3sconf/202564502012

Ridho Fariz, T., Indra Permana, P., Daeni, F., & Putra, A. C. P. (2021). Pemetaan Ekosistem Mangrove di Kabupaten Kubu

Raya Menggunakan Machine Learning pada Google Earth Engine. *Jurnal Geografi : Media Informasi Pengembangan Dan Profesi Kegeografian*, *18*, 83–89. https://doi.org/10.15294/jg.v18i2.30231

Rustiadi, E., Pravitasari, A. E., Setiawan, Y., Mulya, S. P., Pribadi, D. O., & Tsutsumida, N. (2021). Impact of continuous Jakarta megacity urban expansion on the formation of the Jakarta-Bandung conurbation over the rice farm regions. *Cities*, *111*, 103000. https://doi.org/10.1016/j.cities.2020.103000

Seto, K. C., Fragkias, M., Güneralp, B., & Reilly, M. K. (2011). A Meta-Analysis of Global Urban Land Expansion. *PLOS ONE*, *6*(8), e23777. https://doi.org/10.1371/journal.pone.0023777

Seto, K. C., Güneralp, B., & Hutyra, L. R. (2012). Global forecasts of urban expansion to 2030 and direct impacts on biodiversity and carbon pools. *Proceedings of the National Academy of Sciences*, *109*(40), 16083–16088. https://doi.org/10.1073/pnas.1211658109

Sharma, P., Singh, R., & Yogeswaran, N. (2026). Global review of urban heat island research across varied climatic regions. *Discover Environment*, *4*(1), 84. https://doi.org/10.1007/s44274-026-00571-0

Sobrino, J. A., Jiménez-Muñoz, J. C., & Paolini, L. (2004). Land surface temperature retrieval from LANDSAT TM 5. *Remote Sensing of Environment*, *90*(4), 434–440. https://doi.org/10.1016/j.rse.2004.02.003

Stathopoulou, M., & Cartalis, C. (2007). Daytime urban heat islands from Landsat ETM+ and Corine land cover data: An application to major cities in Greece. *Solar Energy*, *81*(3), 358–368. https://doi.org/10.1016/j.solener.2006.06.014

Sukojo, B. M., Rizmasari, N., Hayati, N., Bioresita, F., Audiyana, H., Santoso, E. B., Alimuddin, I., & Hasyim, A. W. (2025). Analysis of Dense Residential Areas Using Normalized Difference Built-Up Index and Its Relation to Land Surface Temperature. *Journal of Human, Earth, and Future*, *6*(2 SE-Research Articles), 371–382. https://doi.org/10.28991/HEF-2025-06-02-08

Suryono, H., Marsuhandi, A. H., & Pramana, S. (2022). Klasifikasi Tutupan Lahan Berdasarkan Random Forest Algorithm Menggunakan Cloud Computing Platform. *Jurnal Aplikasi Statistika & Komputasi Statistik*, *12*(3 SE-Articles), 1–12. https://doi.org/10.34123/jurnalasks.v14i1.383

Takano, T., Morita, H., Nakamura, S., Togawa, T., Kachi, N., Kato, H., & Hayashi, Y. (2023). Evaluating the quality of life for sustainable urban development. *Cities*, *142*, 104561. https://doi.org/10.1016/j.cities.2023.104561

Tiwari, A. K., & Kanchan, R. (2024). Analytical study on the relationship among land surface temperature , land use / land cover and spectral indices using geospatial techniques. *Discover Environment*. https://doi.org/10.1007/s44274-023-00021-1

Viera, A. J., & Garrett, M. J. (2005). Understanding Interobserver Agreement: The Kappa Statistic. *Family Medicine*. https://doi.org/10.1001/jama.268.18.2513

Yamazaki, D., Ikeshima, D., Sosa, J., Bates, P. D., Allen, G. H., & Pavelsky, T. M. (2019). MERIT Hydro: A High-Resolution Global Hydrography Map Based on Latest Topography Dataset. *Water Resources Research*, *55*(6), 5053–5073. https://doi.org/10.1029/2019WR024873